Spatio-temporal Patterns of High Mountain Asia's Snowmelt Season Identified with an Automated Snowmelt Detection Algorithm, 1987-2016

Taylor Smith[1], Bodo Bookhagen[1], and Aljoscha Rheinwalt[1]

[1]Institute for Earth and Environmental Sciences, Universität Potsdam, Germany

Correspondence to: Taylor Smith (tasmith@uni-potsdam.de)

Abstract. High Mountain Asia (HMA), encompassing the Tibetan Plateau and surrounding mountain ranges, is the primary water tower for much of Asia, serving more than a billion downstream users. Many catchments receive the majority of their yearly water budget in the form of snow, which is poorly monitored by sparse in-situ weather networks. Both the timing and volume of snowmelt play critical roles in downstream water provision, as many applications – such as agriculture, drinking-water generation, and hydropower – rely on consistent and predictable snowmelt runoff. Here, we leverage passive microwave data across five sensors (SSMI, SSMIS, AMSR-E, AMSR2, and GPM) from 1987-2016 to track the onset and end of snowmelt across HMA. Compared against a control dataset (n=2100, 3 variables at 25 locations over 28 years), our algorithm is generally within 3-5 days of the onset and end dates of melt. Using the algorithm-generated snowmelt dates, we examine the spatiotemporal patterns of the snowmelt season across HMA. The climatically short (29 year) time series, along with complex inter-annual snowfall variations, makes determining trends in melt onset and end dates at a single point difficult. We instead identify trends in snowmelt timing by using hierarchical clustering of the passive microwave data to determine trends in self-similar regions. We make the following four key observations: (1) The end of the snowmelt season is trending almost universally earlier in HMA (negative trends). Changes in the end of the snowmelt season are generally between 2 and 8 days/decade over the 29-year study period (5 - 25 days total). The length of the snowmelt season is thus shrinking in many, though not all, regions of HMA. Some areas exhibit later snowmelt onset dates (positive trends), but with a generally smaller magnitudes than trends in snowmelt end. (2) Areas with long snowmelt periods, such as the Tibetan Plateau, show the strongest compression of the snowmelt season (negative trends). These trends are apparent regardless of the time period over which the regression is performed. (3) While trends averaged over three decades indicate earlier snowmelt onset and end, data from the last 14 years (2002-2016) exhibit positive trends in both snowmelt onset and end dates in many regions, such as parts of the Pamir and Kunlun Shan. Due to the short nature of the time series, it is not clear whether this change is a reversal in a long-term trend or simply inter-annual variability. (4) Some regions with stable or growing glaciers – such as the Karakoram and Kunlun Shan – see slightly later snowmelt onset and longer snowmelt periods. It is likely that changes in the snowmelt regime of HMA account for some of the observed heterogeneity in glacier response to climate change. While the decadal increases in regional temperature have in general caused earlier snowmelt onset and shortened melt seasons, changes in HMA's crysophere have been spatially and

temporally heterogeneous. The complex response of HMA's cryosphere to climate change highlights the importance of both regional and small-scale studies for effective water planning.

1 Introduction

More than a billion people across Asia rely directly or indirectly on water sourced from melting snow in High Mountain Asia
5 (HMA) (Bookhagen and Burbank, 2010; Bolch et al., 2012; Kääb et al., 2012; Kang et al., 2010; Immerzeel et al., 2010; Gardner et al., 2013; Hewitt, 2005; Malik et al., 2016). Many catchments receive the majority of their yearly water budget in the form of snow – particularly at high elevations (Barnett et al., 2005). Both the volume of snowfall and the timing of snowmelt play crucial roles in the efficacy of water provision for downstream users, as many applications – such as agriculture and hydropower – rely on consistent and predictable water availability. Many areas also rely on snowmelt to provide a water
10 buffer late in the year, when direct precipitation is rare.

Passive microwave (PM) data has been used to estimate snow depth and snow-water equivalent (SWE) since the launch of the Scanning Multichannel Microwave Radiometer (SMMR) in 1978. Consistent, pseudo-daily measurements became available in 1987 with the launch of the Special Sensor Microwave/Imager (SSMI) series of sensors (Wentz, 2013). PM data is highly sensitive to liquid water present in the snowpack, and is thus a valuable tool for tracking the onset of snowmelt across
15 large, inhospitable, and unmonitored regions. PM data also have the advantage of functioning despite cloud cover, which is ubiquitous in much of HMA during the both winter and during the Indian Summer Monsoon (ISM) season. Using satellite-derived PM measurements, several authors have tracked the onset, duration, and spatial extent of snowmelt events using a range of approaches including the cross-polarized gradient ratio (XPGR) (Abdalati and Steffen, 1995; Hall et al., 2004), the advanced horizontal range algorithm (Drobot and Anderson, 2001), Gaussian edge detection (Joshi et al., 2001), channel differ-
20 ences (Takala et al., 2003), artificial neural networks (Takala et al., 2008, 2009), diurnal temperature brightness (Tb) variations (Apgar et al., 2007; Monahan and Ramage, 2010; Tedesco, 2007), and wavelet-based approaches (Liu et al., 2005).

In this study, we adapted a previously published algorithm (Abdalati and Steffen, 1995), which relied on the establishment of a single cutoff threshold for identifying melt phases, to the more complex and diverse snow regimes of HMA. While previous studies have successfully measured snowmelt in large, homogeneous environments such as Greenland and Antarctica, we found
25 these algorithms ineffective in the highly variable topography and snow dynamics of HMA. Here, we present an enhanced and generalized snowmelt algorithm building on previous work to improve on snowmelt detection in HMA. We then apply this algorithm to PM data from 1987-2016, and use the derived melt start and end dates to examine spatio-temporal snowmelt patterns across the entire HMA region.

1.1 Geographic Setting

30 HMA is comprised of several mountain ranges – the Himalaya, Pamir, Karakoram, Hindu Kush, Tien Shan, and Kunlun Shan – which contain the headwaters of major watersheds which serve more than a dozen countries (Fig. 1). Many of these catchments, such as the Tibetan Plateau, Tarim, Syr Darya, Amu Darya, and Indus, rely on snowmelt for more than 50% of their yearly

water budget (Bookhagen and Burbank, 2010; Shrestha et al., 2015). Many communities – particularly those at high elevations or those that depend on surface water for agriculture – are highly reliant on the timing of snowmelt. An early snowmelt season can create a late-season 'water gap' when a dry spell is caused by snow meltwaters disappearing before the start of the next rainy season. These water gaps can also negatively impact flora and fauna which depend heavily on the timing of the appearance

5 of ephemeral water bodies (Bookhagen, 2017). The timing and volume of snowmelt thus has important implications for the environment, direct household water use, agriculture, and hydropower.

Several interacting moisture sources, such as the Winter Westerly Disturbances (WWD), Indian Summer Monsoon (ISM), and East Asian Summer Monsoon (EASM) are responsible for the wide range of snowfall regimes across HMA (Fig. 1, inset). The interaction of these climatic regimes with the complex topography of HMA – particularly the vast elevation gradients –

10 creates a diverse set of snowfall regimes (Cannon et al., 2014; Kääb et al., 2012; Immerzeel and Bierkens, 2012; Gardner et al., 2013; Kapnick et al., 2014; Barnett et al., 2005; Dahe et al., 2006; Takala et al., 2011; Cannon et al., 2017).

2 Materials and Methods

We leverage a combined time series of SSMI (1987-2009), Special Sensor Microwave Imager/Sounder (SSMIS) (2008-2016), Advanced Microwave Scanning Radiometer - Earth Observing System (AMSR-E, 2002-2011), AMSR2 (2012-2016), and

15 Global Precipitation Measurement (GPM, 2014-2016) data, processed to 0.25 decimal degree (dd) resolution by interpolating raw PM swath data at a series of point locations as described in Smith and Bookhagen (2016) (see Supplementary Table 1 for a full dataset listing). In essence, we group all measurements within a $0.125°$ dd radius of each point on a $0.25°$ dd grid and generate a spatially weighted mean value for each swath at that point. The dataset is comprised of 6,399 point locations, with on average 26,000 PM measurements each (long-term average of 2.4 measurements/day for 29 years, with more measurements

20 during the 2002-2016 period).

2.1 Snowmelt Tracking Algorithm

The shift from dry snow, which can be physically characterized as snow crystals in an air background, to wet snow, which replaces the air matrix with water, shifts the primary interaction between PM radiation and the snowpack from volumetric (dry snow) to surface (wet snow) scattering. These scattering changes are reflected in the temperature brightness (Tb) data, and

25 allow wet and dry snow to be differentiated. The XPGR, as originally described by Abdalati and Steffen (1995), is defined as:

$$XPGR = (Tb_{19H} - Tb_{37V})/(Tb_{19H} + Tb_{37V}) \qquad (1)$$

This algorithm takes advantage of both the channel difference between the Tb_{19} and Tb_{37} GHz channels as well as the depolarization effects of snowmelt, which increases the differences between the horizontally and vertically polarized channels (Abdalati and Steffen, 1995). As this algorithm is normalized, it does not require ground calibration data, which is advantageous

in HMA. Snowmelt onset can be determined using either a static or dynamic threshold. In the original application of the XPGR on the Greenland Ice Sheet, a static value of -0.025 was used to detect snowmelt (Abdalati and Steffen, 1995).

We find that for the majority of HMA, the -0.025 threshold is much too low to effectively detect melt. Indeed, the yearly peak XPGR is highly variable throughout time and space, and a constant threshold was found to be inappropriate for HMA.

5 Additionally, while the XPGR time series is effective for tracking the onset of snowmelt, it is not effective for tracking the cessation of snowmelt. To track the end of snowmelt, we leverage two additional datasets: (1) the raw Tb_{37V} time series, which rapidly increases as snowpack thins, and (2) a SWE time series calculated from the Tb_{19} and Tb_{37} GHz channels (Chang et al., 1987; Kelly et al., 2003; Tedesco et al., 2015; Smith and Bookhagen, 2016).

We first use a simple peak-finding algorithm, which identifies peaks as points which are larger than their two neighboring

10 samples, to generate a list of potential peaks in the XPGR data. Next, we take the average XPGR value within $\pm$ 3 days of each peak to determine not only the simple yearly maximum XPGR, but the highest and temporally widest peak in our XPGR data.

To determine the end of the snowmelt season, we choose either the date of the yearly maximum Tb_{37V} value, which corresponds to the thinnest snowpack or to a 'bare earth' signal, or the first date where 4 out of 5 days have been within 2 cm of the yearly SWE minimum. We choose the yearly SWE minimum instead of zero as our SWE threshold for snow clearance

15 because some regions in HMA have a defined melt season but rarely reach zero SWE. This also helps control for uncertainty in shallow SWE measurements, as detecting shallow snow (<5 cm) with PM data is still difficult (Kelly et al., 2003; Armstrong and Brodzik, 2001). A full description of our melt detection algorithm is available in the Supplement (Figure S1).

2.2 Manual Control Dataset Generation

Unfortunately, large-scale and several-decades long snowmelt onset and end date records are not available for HMA. Instead,

20 we use a manually generated set of control dates for the onset and end of snowmelt, determined from the SWE, XPGR, and Tb_{37V} signals by the researchers. We visually identified major peaks, as well as the cessation of snowmelt, by inspection of the time series. We chose a random sample of 25 point locations across our study area, and identify start and end dates for each year of the time series (n=1400). We use the calculated length of the snowmelt period as an additional control variable (n=700).

2.3 Hierarchical Clustering

25 Hierarchical clustering is a method used to correlate time series data by intrinsic similarity (Corpet, 1988; Johnson, 1967; Jain et al., 1999; Murtagh and Contreras, 2012; Rheinwalt et al., 2015), which has been used extensively in the environmental research community. We generate clusters from those time series which share the most temporal overlap, or where the periodicity of Tb values have the largest coherence, regardless of their spatial correlation.

We choose the XPGR time series as our clustering variable, as the XPGR is the most sensitive to melt dynamics, integrates

30 multiple Tb frequencies, and is not sensitive to SWE calibration issues. To improve the robustness of our clustering, we combine the disparate single-instrument PM time series into a single coherent time series which leverages the full temporal extent of each dataset (1987-2016), using the following three steps: (1) We standardize the PM signals of the suite of instruments used in this study to a single set of dates, artificially created at daily resolution from the minimum and maximum dates across all

satellite datasets, by resampling all individual satellite time series to a daily time step and dropping dates without data. (2) We regularize the disparate PM time series based on the overlapping portions of individual satellite time series, using linear regression. The results of these regressions can be seen in Table S2, with an example regression at a single point shown in Figure 2. (3) In order to reduce noise in our cluster analysis, we resample our merged XPGR time series to a 5-day temporal

5   resolution (pentad).

Next, we normalize each merged pentad time series (1987-2016) to a Gaussian distribution, using a percentile mapping approach (Rheinwalt, 2017). We then estimate the Pearson correlation coefficient to classify regions of self-similarity in our XPGR time series (Rheinwalt, 2016). This method computes a Pearson correlation coefficient between each time series, and based on the resulting correlation matrix, computes a set of linkages using the angle between time series in vector space

10   (Murtagh and Contreras, 2012). We use the maximum distance (complete linkage) to split the linkage matrix, which is favorable because it ensures a minimum intra-cluster correlation. An average linkage scheme was tested and produced heterogeneous cluster sizes with outliers. We choose our cluster threshold from the hierarchical clustering dendrogram (Figure S2) which maximizes cluster size while minimizing cluster internal diversity (Figure S3). We emphasize that the correlation is based on the temporal co-evolution of the time series, and is less sensitive to the relative magnitudes of peaks and troughs between data

15   points. For an oscillating time series, the magnitude of the Pearson correlation coefficient is driven by the synchronization of peak timing, especially in normalized time series. The combination of several sensors in this study may impact the magnitudes of the resultant time series, but will not have an outsized effect on the timing, and thus clustering, of our time series.

3   Results

3.1   Melt Algorithm Validation

20   The agreement between manually clicked start/end dates and algorithm-derived start/end dates is generally within 3 days, with more than 70% of start and end dates falling within 5 days of the control dataset (Table 1). We find the lowest standard deviation for the end of melt, which is to be expected given that the end of snowmelt is determined by both snow clearance and the Tb_{37V} signal, and thus is more tightly constrained than the melt onset date. The melt onset date, while having a low average offset, has a high standard deviation as the algorithm sometimes has trouble correctly choosing the onset of melt when a snow season

25   has several large storms, or several periods of melting and refreezing (cf. Fig. 3). Thus, errors in identification of melt onset will naturally have a higher standard deviation due to the presence of more relatively large misclassification errors.

Diverse snow seasons are shown from an example location (71.25E, 36.75N), over four years of data (Fig. 3). Despite clear inter-annual variations in the temporal distribution of SWE, there exists high correlation between the algorithm-derived melt dates and our manually chosen melt dates. In the sample data, the first shown snow season has a simple structure with a

30   well-defined peak and a pseudo-linear melt during the spring season. The second year of data has a small melt pulse in the spring, followed by a large increase of SWE, causing a two-peaked SWE distribution. The third year has several small SWE peaks throughout the winter and spring, corresponding to phases of snowfall and brief periods of snowmelt. The final year of data shown has a two-peaked SWE distribution, but the late-season storm does not deposit more snow than the early-season

maximum. Despite drastic differences in SWE regimes between years, the main melt phase start and end dates were generally correctly identified (Fig. 3).

3.2 Application: Spatial Patterns of Snowmelt Period

Using our melt tracking algorithm, we can identify the start and end dates of melt on a yearly basis. This also allows us to
5   calculate the length of the snowmelt season, termed here the snowmelt period. The long-term average snowmelt period is shown in Figure 4.

The length of the snowmelt season varies significantly across HMA (Fig. 5). In many low-elevation areas, such as the Ganges Plain, and low-SWE areas, such as the central Tarim Basin, snow is present for less than a month on average. Higher-elevation zones, and in particular the Tibetan Plateau, see melt periods of several months. While both elevation and the amount of SWE
10   impact snowmelt, these are not the sole determinants of snowmelt onset and end (Fig. 5). Each of the major catchments (cf. Fig. 1) has a unique melt start date, end date, and snowmelt-period distribution, based on the various climate and topographic forcings present in each catchment.

3.3 Hierarchical Clusters

Cluster selection criteria can be seen in Figures S2-3. We base our selected dendrogram cutoff (distance threshold in vector
15   space) on a combination of the number of generated clusters, the internal variation within those clusters, and the average resultant cluster size. In our case, we choose a distance cutoff of 1 radian from the complete linkage matrix (minimum intra-cluster correlation 0.525), which results in 285 clusters (Fig. 6).

While the hierarchical clusters are not based on any explicit spatial relationships, many of the clusters fall into spatially coherent groups. For example, the Pamir Knot and Tarim basin both form large, coherent clusters based on the similarity of
20   their snowfall and snowmelt patterns. The large number of small clusters throughout the Himalaya indicate that the region is not climatically uniform, and small-scale variations in topography and climate have strong impacts on the snowmelt regime.

4 Discussion

4.1 Spatial Melt Patterns from Hierarchical Clustering

As can be seen in Figure 3, inter-annual variation in snowfall can cause large disparities in the yearly dates of snowmelt onset
25   and end. This is particularly true of areas impacted by the WWD, which often have multiple snowfall events starting in winter and lasting until spring (Cannon et al., 2014). This complicates change detection of the onset of melt between years, as one year may receive a small late season storm, and thus start the major snowmelt phase in the spring, while the next year may receive a large summer storm, and thus start its main snowmelt phase in the summer.

To mitigate the influence of inter-annual variation in determining long-term trends in snowmelt onset and end, we group
30   our data into self-similar clusters using hierarchical clustering. We do not filter our generated clusters based on size or self-

similarity, as we do not use our clusters to generate a single averaged or representative time series for each cluster, as is often done in climate analyses. Due to inter-annual variations in SWE, and snowmelt onset/end dates, fitting a linear regression through only 29 years of data does not provide statistically significant results for the majority of HMA. Instead, we use our clusters to group sets of algorithmically-derived melt onset and end dates, and fit linear models on a cluster-by-cluster basis. By leveraging the melt start and end dates of a set of time series in parallel, we are able to identify statistically significant changes in melt onset and end dates, as well as changes in the length of the snowmelt period (Fig. 7). To reduce noise from low-SWE and very short snowmelt period areas, we remove areas from the subsequent analyses with long-term average melt periods of less than 20 days.

Changes in snowmelt onset date are split between earlier melt onset (negative trend) outside of the Tibetan Plateau, and slightly later onset (positive trend) in many high elevation areas running from the Karakoram through the Tibetan Plateau (Fig. 7A). Negative snowmelt onset trends have been previously observed in Central Asia (Lioubimtseva and Henebry, 2009; Dietz et al., 2014) and the Himalaya (Lau et al., 2010; Panday et al., 2011), but have not been confirmed a with decadal-timescale, large-area and empirical study of snowmelt dates.

Increasing spring snow depth has been observed across the Tibetan Plateau since the 1970s (Zhang et al., 2004; Che et al., 2008), which could help account for the later onset observed in the majority of the Tibetan Interior. High-elevation zones in the upper Indus catchment, running from the Karakorum in a south-eastward direction, have seen increased precipitation over the past decades due to increases in the strength of the WWD (Cannon et al., 2015; Norris et al., 2016; Treydte et al., 2006). Changes in the eastern Himalaya are likely driven by a combination of late season storms, increased snowfall over the past decades, and the very high average elevation of this region (Stewart, 2009).

Temperatures in HMA are increasing faster than the global average (Vaughan et al., 2013; Lau et al., 2010), and are likely the primary driver of the almost universal earlier snowmelt end dates as seen in Figure 7B. Increased temperatures have likely both reduced overall SWE amounts, by causing more precipitation to fall as rain, and decreased SWE persistence into the spring and summer months. These changes have helped drive a 2-8 day/decade earlier end to the snowmelt season (Fig. 7B).

The length of the snowmelt season is shortening in much of HMA, with the exception of an area running from the Pamir to Kunlun Shan (Fig. 7C). We attribute this to a combination of increased storm intensity in the WWD, and increases in late season storms, which could help extend the snowmelt season slightly later into the year (Cannon et al., 2016; Norris et al., 2015; Kapnick et al., 2014). In general, however, the snowmelt season is shortening throughout HMA. Intensification of the spring runoff regime in HMA has been observed in both model (Lutz et al., 2014) and empirical (Dietz et al., 2014; Bookhagen and Burbank, 2010; Stewart, 2009) data.

4.2 Temporal Heterogeneity in Snowmelt Trends

Not only are changes in the snowmelt regime spatially complex (e.g., Fig. 7), but they exhibit distinct temporal heterogeneity as well.

Changes in snowmelt onset do not have a bias towards early or late onset snow regimes (Fig. 8). The end of the snowmelt season is almost universally negative (earlier), excepting a few early-onset zones. These zones are predominantly low-SWE,

short melt-season, areas (cf. Fig. 7). The majority of locations show negative (shorter) trends in snowmelt period. Strong negative changes in the snowmelt period are biased towards areas with long melt seasons (120 days or more). This implies that high-elevation areas, such as the Tibetan Plateau, and high-SWE areas, such as the Karakoram, will see a relatively stronger compression in the length of the snowmelt season. While changes in the snowmelt onset date are partially responsible, the main

5   driver of shorter snowmelt periods is the earlier end of the snowmelt season across most of HMA.

Several-decade long trends conceal short-term fluctuations in the snowmelt regime of HMA. To assess the impact of the analysis timeframe on our regression results, we analyzed trends with window sizes ranging from four years to 28 years, across all possible start-year and window-size combinations, averaged over the entire study area (Fig. 9).

Trends are universally negative for the onset and end of the snowmelt season, as well as for the snowmelt period, between

10   1988 and 1995, regardless of the timeframe over which the regression is performed. While there were some short positive trends in snowmelt end date (5-10 years) starting in the mid 1990s, trends in end dates and snowmelt period are generally negative. Although long-term trends in snowmelt onset date (longer than 20 years) are negative, recent trends (after 2002) in snowmelt onset date are positive when considered at timeframes of 5-10 years. This implies that while the three-decade trend in snowmelt onset dates has been negative, the trend has become more variable in the past decade.

15   It is clear that decadal trends (cf. Fig. 7) are not consistent throughout the entire study period (cf. Fig. 9). When trends in the first half (1988-2002) and second half (2002-2016) of the data are compared, distinct regional patterns are apparent (Fig. 10).

The lack of statistically significant trends limits some interpretations, particularly with regards to changes in the snowmelt period. Only small parts of the Tibetan Plateau and the eastern Himalaya have maintained trends towards later snowmelt onset through both analysis periods. While many snowmelt end dates have remained negative in both time periods, trends in parts of

20   the Pamir and Karakoram have moved from negative to positive, and those in the Tien Shan have become less negative (cf Fig. S4). A similar story is apparent when snowmelt onset dates are considered, where the Tien Shan and parts of the Pamir have moved from negative to positive snowmelt onset dates. Unfortunately, due the the climatically short nature of the dataset, it is not clear whether this change represents inter-annual variability or a reversal of a long-term trend.

4.3   Hydrologic Implications

25   The spatially and topographically complex changes in snowmelt onset, end, and period make interpretation of downstream impacts difficult. The long-term trend in HMA of a shortened and earlier melt season will impact downstream populations who rely on the consistent timing and volume of spring and summer runoff (Archer and Fowler, 2004; Barnett et al., 2005). Already the impacts of precipitation intensification and shifts in the snowmelt season have been felt in many regions (Barnett et al., 2005; Stewart, 2009). These trends are likely to continue as temperatures rise across HMA, and each major catchment will feel

30   the impacts of a shortened snowmelt season, regardless of changes in the start and end dates of melt.

Many regions rely on glaciers as their only water source between the end of snowmelt and the beginning of major precipitation systems (Bolch et al., 2012). This important water reserve is certain to be impacted by, and reflect changes in, the snowmelt regime of HMA, as the timing of precipitation has been shown to be an important factor in the response of glaciers to climate change (Maussion et al., 2014; Wang et al., 2017). While many regions have seen rapid glacier retreat (Bolch et al., 2012;

Kääb et al., 2012, 2015; Scherler et al., 2011) there exist regions of glacier stability and even growth, such as the Karakoram (Hewitt, 2005; Gardelle et al., 2012) and Kunlun Shan (Gardner et al., 2013; Yao et al., 2012). Our results (cf. Fig. 7) show longer snowmelt periods in parts of the Pamir and Kunlun Shan, later snowmelt onset in parts of the Karakoram and Kunlun Shan, and relatively less negative trends in snowmelt end in the Pamir, Karakoram, and Kunlun Shan when compared with the rest of HMA. These regions overlap with both the 'Karakoram Anomaly' and positive glacier mass balances in parts of the Kunlun Shan and Pamir, implying that changes in the timing of the snowmelt season could be partially responsible for regional heterogeneity in glacier change.

The majority of HMA, however, exhibits a three-decade long trend towards an earlier end of the snowmelt season. Earlier snow clearance increases the absorption of solar radiation, and thus stores more heat at high elevations and generates a positive feedback (Willis et al., 2002). As seasonal snow is removed earlier from glacier regions, glacier melt will accelerate. In general, glaciers in HMA are shrinking, which fits with the observed long-term decrease in snowmelt end dates (cf. Figs. 7, 8, 9), despite clear spatial and temporal heterogeneity in these trends (cf. Fig. 10).

5 Conclusions

This study presents a snowmelt tracking algorithm based on the cross-polarized gradient ratio, native passive microwave (PM) signal, and a rough estimate of snow-water equivalent (SWE). We do not rely on static thresholds to determine the onset or end of the snowmelt season across our diverse study region, but instead rely on identifying the snowmelt signal from intrinsic properties of each individual time series. The algorithm leverages passive microwave data from the Special Sensor Microwave/Imager (SSMI), Special Sensor Microwave Imager/Sounder (SSMIS), Advanced Microwave Scanning Radiometer - Earth Observing System (AMSR-E), AMSR2, and Global Precipitation Measurement (GPM) satellites (1987-2016) to track the onset, duration, and end of the snowmelt season across High Mountain Asia (HMA). We examine large-scale spatial patterns in the snowmelt regime and identify trends in the timing of snowmelt across HMA over the past three decades using hierarchical clustering.

We find the following four key points: (1) The snowmelt season is ending earlier in much of HMA (negative trend), with magnitudes between 2 and 8 days/decade (5-25 days total over 29 years). The length of the snowmelt season is shortening in the majority of HMA, despite some regions of delayed snowmelt onset. (2) Negative changes to the end of the snowmelt season are felt most strongly in areas with long snowmelt seasons (as averaged over three decades), such as the Tibetan Plateau and high-SWE areas in the Himalaya, Karakoram, and Tien Shan. (3) While three-decade long trends indicate earlier start and end dates for the snowmelt season, recent (2002-2016) trends are positive (later) in many regions of HMA. These changes could be due to inter-annual variability or a reversal in the long-term trend. (4) Areas with slightly longer snowmelt seasons or later onset dates overlap with regions of positive glacier mass balance, such as the Karakoram and Kunlun Shan. This implies that changes to the snowmelt regime of HMA could help account for some of the observed regional glacier changes. In general, however, regional warming has caused long-term earlier snowmelt onset and shortened melt seasons in much of HMA. These

changes are spatially and temporally complex, and will require further local and high-spatial resolution assessments to fully understand changes in HMA's cryosphere.

Code availability. The code used in this study is available online at: https://github.com/UP-RS-ESP/SnowmeltTracking

Author contributions. T.S. and B.B. designed the study, T.S. prepared and analyzed the PM data. B.B. and A.R. contributed to the develop-
5 ment of the methodology. T.S. wrote the manuscript with input from all authors.

Competing interests. The authors declare that they have no conflict of interest.

References

Abdalati, W. and Steffen, K.: Passive microwave-derived snow melt regions on the Greenland Ice Sheet, Geophysical Research Letters, 22, 787–790, 1995.

Apgar, J. D., Ramage, J. M., McKenney, R. A., and Maltais, P.: AMSR-E algorithm for snowmelt onset detection in sub-arctic heterogeneous terrain, Hydrological processes, 21, 1587–1596, 2007.

Archer, D. R. and Fowler, H.: Spatial and temporal variations in precipitation in the Upper Indus Basin, global teleconnections and hydrological implications, Hydrology and Earth System Sciences Discussions, 8, 47–61, 2004.

Armstrong, R. and Brodzik, M.: Recent Northern Hemisphere snow extent: A comparison of data derived from visible and microwave satellite sensors, Geophysical Research Letters, 28, 3673–3676, 2001.

Barnett, T. P., Adam, J. C., and Lettenmaier, D. P.: Potential impacts of a warming climate on water availability in snow-dominated regions, Nature, 438, 303–309, 2005.

Bolch, T., Kulkarni, A., Kääb, A., Huggel, C., Paul, F., Cogley, J., Frey, H., Kargel, J., Fujita, K., Scheel, M., et al.: The state and fate of Himalayan glaciers, Science, 336, 310–314, 2012.

Bookhagen, B.: Chapter 11: The influence of Hydrology and Glaciology on Wetlands in the Himalaya, in: Bird Migration Across the Himalayas: Wetland Functioning Amidst Mountains and Glaciers, edited by Prins, H. and Namgail, T., Cambridge University press, 2017.

Bookhagen, B. and Burbank, D. W.: Toward a complete Himalayan hydrological budget: Spatiotemporal distribution of snowmelt and rainfall and their impact on river discharge, Journal of Geophysical Research: Earth Surface (2003–2012), 115, 2010.

Cannon, F., Carvalho, L., Jones, C., and Bookhagen, B.: Multi-annual variations in winter westerly disturbance activity affecting the Himalaya, Climate Dynamics, pp. 1–15, 2014.

Cannon, F., Carvalho, L. M., Jones, C., and Norris, J.: Winter westerly disturbance dynamics and precipitation in the western Himalaya and Karakoram: a wave-tracking approach, Theoretical and Applied Climatology, pp. 1–18, 2015.

Cannon, F., Carvalho, L., Jones, C., Hoell, A., Norris, J., Kiladis, G., and Tahir, A.: The influence of tropical forcing on extreme winter precipitation in the western Himalaya, Climate Dynamics, 2016.

Cannon, F., Carvalho, L. M. V., Jones, C., Norris, J., Bookhagen, B., and Kiladis, G. N.: Effects of Topographic Smoothing on the Simulation of Winter Precipitation in High Mountain Asia, Journal of Geophysical Research: Atmospheres, pp. n/a–n/a, doi:10.1002/2016JD026038, http://dx.doi.org/10.1002/2016JD026038, 2016JD026038, 2017.

Chang, A., Foster, J., and Hall, D.: Nimbus-7 SMMR derived global snow cover parameters, Annals of glaciology, 9, 39–44, 1987.

Che, T., Xin, L., Jin, R., Armstrong, R., and Zhang, T.: Snow depth derived from passive microwave remote-sensing data in China, Annals of Glaciology, 49, 145–154, 2008.

Corpet, F.: Multiple sequence alignment with hierarchical clustering, Nucleic acids research, 16, 10 881–10 890, 1988.

Dahe, Q., Shiyin, L., and Peiji, L.: Snow cover distribution, variability, and response to climate change in western China, Journal of climate, 19, 1820–1833, 2006.

Dietz, A. J., Conrad, C., Kuenzer, C., Gesell, G., and Dech, S.: Identifying changing snow cover characteristics in Central Asia between 1986 and 2014 from remote sensing data, Remote Sensing, 6, 12 752–12 775, 2014.

Drobot, S. D. and Anderson, M. R.: An improved method for determining snowmelt onset dates over Arctic sea ice using scanning multi-channel microwave radiometer and Special Sensor Microwave/Imager data, 2001.

Gardelle, J., Berthier, E., and Arnaud, Y.: Slight mass gain of Karakoram glaciers in the early twenty-first century, Nature geoscience, 5, 322–325, 2012.

Gardner, A. S., Moholdt, G., Cogley, J. G., Wouters, B., Arendt, A. A., Wahr, J., Berthier, E., Hock, R., Pfeffer, W. T., Kaser, G., et al.: A reconciled estimate of glacier contributions to sea level rise: 2003 to 2009, Science, 340, 852–857, 2013.

5 Hall, D. K., Williams Jr, R. S., Steffen, K., and Chien, J. Y.: Analysis of summer 2002 melt extent on the Greenland Ice Sheet using MODIS and SSM/I data, in: Geoscience and Remote Sensing Symposium, 2004. IGARSS'04. Proceedings. 2004 IEEE International, vol. 5, pp. 3029–3032, IEEE, 2004.

Hewitt, K.: The Karakoram anomaly? Glacier expansion and the'elevation effect,'Karakoram Himalaya, Mountain Research and Development, 25, 332–340, 2005.

10 Immerzeel, W. and Bierkens, M.: Asia's water balance, Nature Geoscience, 5, 841–842, 2012.

Immerzeel, W. W., Van Beek, L. P., and Bierkens, M. F.: Climate change will affect the Asian water towers, Science, 328, 1382–1385, 2010.

Jain, A. K., Murty, M. N., and Flynn, P. J.: Data clustering: a review, ACM computing surveys (CSUR), 31, 264–323, 1999.

Johnson, S. C.: Hierarchical clustering schemes, Psychometrika, 32, 241–254, 1967.

Joshi, M., Merry, C. J., Jezek, K. C., and Bolzan, J. F.: An edge detection technique to estimate melt duration, season and melt extent on the

15 Greenland ice sheet using passive microwave data, Geophysical Research Letters, 28, 3497–3500, 2001.

Kääb, A., Berthier, E., Nuth, C., Gardelle, J., and Arnaud, Y.: Contrasting patterns of early twenty-first-century glacier mass change in the Himalayas, Nature, 488, 495–498, 2012.

Kääb, A., Treichler, D., Nuth, C., and Berthier, E.: Brief Communication: Contending estimates of 2003–2008 glacier mass balance over the Pamir–Karakoram–Himalaya, The Cryosphere, 9, 557–564, 2015.

20 Kang, S., Xu, Y., You, Q., Flügel, W.-A., Pepin, N., and Yao, T.: Review of climate and cryospheric change in the Tibetan Plateau, Environmental Research Letters, 5, 015 101, 2010.

Kapnick, S. B., Delworth, T. L., Ashfaq, M., Malyshev, S., and Milly, P.: Snowfall less sensitive to warming in Karakoram than in Himalayas due to a unique seasonal cycle, Nature Geoscience, 7, 834–840, 2014.

Kelly, R. E., Chang, A. T., Tsang, L., and Foster, J. L.: A prototype AMSR-E global snow area and snow depth algorithm, Geoscience and

25 Remote Sensing, IEEE Transactions on, 41, 230–242, 2003.

Lau, W. K., Kim, M.-K., Kim, K.-M., and Lee, W.-S.: Enhanced surface warming and accelerated snow melt in the Himalayas and Tibetan Plateau induced by absorbing aerosols, Environmental Research Letters, 5, 025 204, 2010.

Lioubimtseva, E. and Henebry, G. M.: Climate and environmental change in arid Central Asia: Impacts, vulnerability, and adaptations, Journal of Arid Environments, 73, 963–977, 2009.

30 Liu, H., Wang, L., and Jezek, K. C.: Wavelet-transform based edge detection approach to derivation of snowmelt onset, end and duration from satellite passive microwave measurements, International Journal of Remote Sensing, 26, 4639–4660, 2005.

Lutz, A., Immerzeel, W., Shrestha, A., and Bierkens, M.: Consistent increase in High Asia's runoff due to increasing glacier melt and precipitation, Nature Climate Change, 4, 587–592, 2014.

Malik, N., Bookhagen, B., and Mucha, P. J.: Spatiotemporal patterns and trends of Indian monsoonal rainfall extremes, Geophysical Research

35 Letters, 43, 1710–1717, 2016.

Maussion, F., Scherer, D., Mölg, T., Collier, E., Curio, J., and Finkelnburg, R.: precipitation seasonality and variability over the Tibetan Plateau as resolved by the High Asia Reanalysis*, Journal of Climate, 27, 1910–1927, 2014.

Monahan, P. A. and Ramage, J.: AMSR-E melt patterns on the Southern Patagonia Icefield, Journal of Glaciology, 56, 699–708, 2010.

Murtagh, F. and Contreras, P.: Algorithms for hierarchical clustering: an overview, Wiley Interdisciplinary Reviews: Data Mining and Knowledge Discovery, 2, 86–97, 2012.

Norris, J., Carvalho, L. M., Jones, C., and Cannon, F.: WRF simulations of two extreme snowfall events associated with contrasting extratropical cyclones over the western and central Himalaya, Journal of Geophysical Research: Atmospheres, 120, 3114–3138, 2015.

Norris, J., Carvalho, L. M., Jones, C., Cannon, F., Bookhagen, B., Palazzi, E., and Tahir, A. A.: The spatiotemporal variability of precipitation over the Himalaya: evaluation of one-year WRF model simulation, Climate Dynamics, pp. 1–26, 2016.

Panday, P. K., Frey, K. E., and Ghimire, B.: Detection of the timing and duration of snowmelt in the Hindu Kush-Himalaya using QuikSCAT, 2000–2008, Environmental Research Letters, 6, 024 007, 2011.

Rheinwalt, A.: Python C-extension for memory efficient and multithreaded Pearson product-moment correlation coefficient estimation using OpenMP, https://github.com/UP-RS-ESP/CorrCoef, 2016.

Rheinwalt, A.: Normalize time series by quantile normalization to the normal distribution., https://github.com/UP-RS-ESP/CorrCoef, https://github.com/UP-RS-ESP/Normalize, 2017.

Rheinwalt, A., Goswami, B., Boers, N., Heitzig, J., Marwan, N., Krishnan, R., and Kurths, J.: Teleconnections in Climate Networks: A Network-of-Networks Approach to Investigate the Influence of Sea Surface Temperature Variability on Monsoon Systems, in: Machine Learning and Data Mining Approaches to Climate Science, pp. 23–33, Springer, 2015.

Scherler, D., Bookhagen, B., and Strecker, M. R.: Spatially variable response of Himalayan glaciers to climate change affected by debris cover, Nature Geoscience, 4, 156–159, 2011.

Shrestha, M., Koike, T., Hirabayashi, Y., Xue, Y., Wang, L., Rasul, G., and Ahmad, B.: Integrated simulation of snow and glacier melt in water and energy balance-based, distributed hydrological modeling framework at Hunza River Basin of Pakistan Karakoram region, Journal of Geophysical Research: Atmospheres, 120, 4889–4919, 2015.

Smith, T. and Bookhagen, B.: Assessing uncertainty and sensor biases in passive microwave data across High Mountain Asia, Remote Sensing of Environment, 181, 174–185, 2016.

Stewart, I. T.: Changes in snowpack and snowmelt runoff for key mountain regions, Hydrological Processes, 23, 78–94, 2009.

Takala, M., Pulliainen, J., Huttunen, M., and Hallikainen, M.: Estimation of the beginning of snow melt period using SSM/I data, in: Geoscience and Remote Sensing Symposium, 2003. IGARSS'03. Proceedings. 2003 IEEE International, vol. 4, pp. 2841–2843, IEEE, 2003.

Takala, M., Pulliainen, J., Huttunen, M., and Hallikainen, M.: Detecting the onset of snow-melt using SSM/I data and the self-organizing map, International Journal of Remote Sensing, 29, 755–766, 2008.

Takala, M., Pulliainen, J., Metsämäki, S. J., and Koskinen, J. T.: Detection of snowmelt using spaceborne microwave radiometer data in Eurasia from 1979 to 2007, Geoscience and Remote Sensing, IEEE Transactions on, 47, 2996–3007, 2009.

Takala, M., Luojus, K., Pulliainen, J., Derksen, C., Lemmetyinen, J., Kärnä, J.-P., Koskinen, J., and Bojkov, B.: Estimating northern hemisphere snow water equivalent for climate research through assimilation of space-borne radiometer data and ground-based measurements, Remote Sensing of Environment, 115, 3517–3529, 2011.

Tedesco, M.: Snowmelt detection over the Greenland ice sheet from SSM/I brightness temperature daily variations, Geophysical Research Letters, 34, 2007.

Tedesco, M., Derksen, C., Deems, J. S., and Foster, J. L.: Remote sensing of snow depth and snow water equivalent, Remote Sensing of the Cryosphere, pp. 73–98, 2015.

Treydte, K. S., Schleser, G. H., Helle, G., Frank, D. C., Winiger, M., Haug, G. H., and Esper, J.: The twentieth century was the wettest period in northern Pakistan over the past millennium, Nature, 440, 1179–1182, 2006.

Vaughan, D., Comiso, J., Allison, I., Carrasco, J., Kaser, G., Kwok, R., Mote, P., Murray, T., Paul, F., Ren, J., Rignot, E., Solomina, O., Steffen, K., and Zhang, T.: Observations: Cryosphere. In: Climate Change 2013: The Physical Science Basis., Contribution of Working Group I to the Fifth Assessment Report of the IPCC., 2013.

Wang, Q., Yi, S., and Sun, W.: Precipitation-driven glacier changes in the Pamir and Hindu Kush mountains, Geophysical Research Letters, pp. n/a–n/a, doi:10.1002/2017GL072646, http://dx.doi.org/10.1002/2017GL072646, 2017.

Wentz, F. J.: SSM/I version-7 calibration report, Remote Sensing Systems Rep, 11012, 46, 2013.

Willis, I. C., Arnold, N. S., and Brock, B. W.: Effect of snowpack removal on energy balance, melt and runoff in a small supraglacial catchment, Hydrological Processes, 16, 2721–2749, doi:10.1002/hyp.1067, http://dx.doi.org/10.1002/hyp.1067, 2002.

Yao, T., Thompson, L., Yang, W., Yu, W., Gao, Y., Guo, X., Yang, X., Duan, K., Zhao, H., Xu, B., et al.: Different glacier status with atmospheric circulations in Tibetan Plateau and surroundings, Nature Climate Change, 2, 663–667, 2012.

Zhang, Y., Li, T., and Wang, B.: Decadal change of the spring snow depth over the Tibetan Plateau: the associated circulation and influence on the east Asian summer monsoon*, Journal of Climate, 17, 2780–2793, 2004.

Table 1. Summary statistics comparing the manual control dataset and the algorithm dataset (n=2100, 28 snowmelt seasons at 25 locations).

Variable	Mean Offset (days)	Mean Absolute Offset (days)	Standard Deviation	RMSE	Percentage of Algorithm Dates Within 3/5/10 Days of Control Dates
Snowmelt Onset	0.98	6.82	19.22	19.25	71 / 77 / 87 %
Snowmelt End	-0.70	4.70	9.82	9.84	57 / 74 / 87 %
Snowmelt Period	-1.61	9.98	21.08	21.14	46 / 61 / 75 %
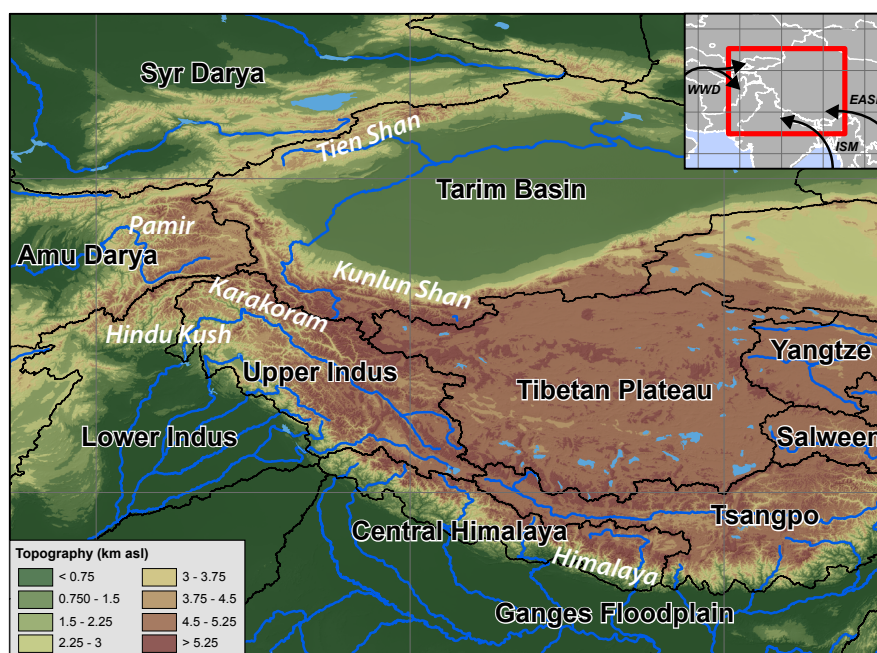
Figure 1. Topographic map of the study area across High Mountain Asia (HMA), with major catchment boundaries (black lines and labels in black font with white border) and major mountain ranges (white font). Inset map shows wind direction of major Asian weather systems (WWD: Winter Westerly Disturbances, ISM: Indian Summer Monsoon, EASM: East Asian Summer Monsoon) on top of political boundaries.
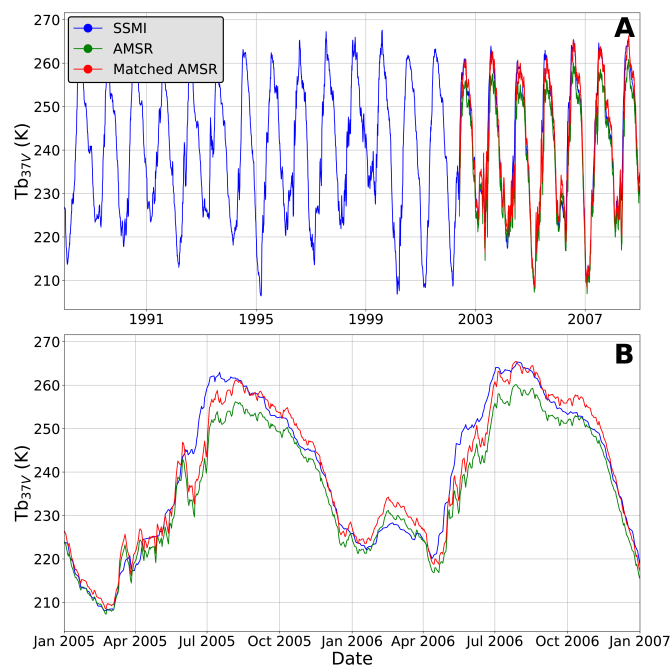
Figure 2. (a) Sample time series showing SSMI (blue) and AMSR-E (green) Tb_{37V} frequencies, with linearly matched modified AMSR-E Tb (red), 1987-2009. Data taken from 71.25E, 36.75N. (b) The same data as panel A but for two seasons (2005-2007).
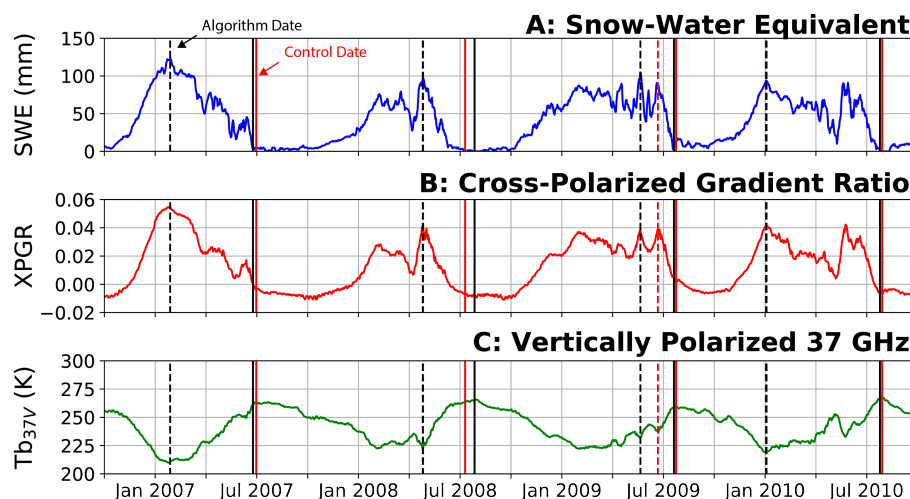
Figure 3. Sample data from 71.25E, 36.75N showing: (a) Snow-Water Equivalent (SWE) based on the Chang algorithm (Chang et al., 1987), (b) Cross-Polarized Gradient Ratio (XPGR), and (c) vertically polarized temperature brightness at 37 GHz (Tb_{37V}) measurements. Onset of melt (dashed lines) and end of melt (solid lines) are black for algorithm dates, and red for control dates. Lack of red lines indicates temporal overlap of algorithm and control dates. We use the XPGR to identify the start of melt, and the SWE and Tb_{37V} measurements to identify the end of the melt season.
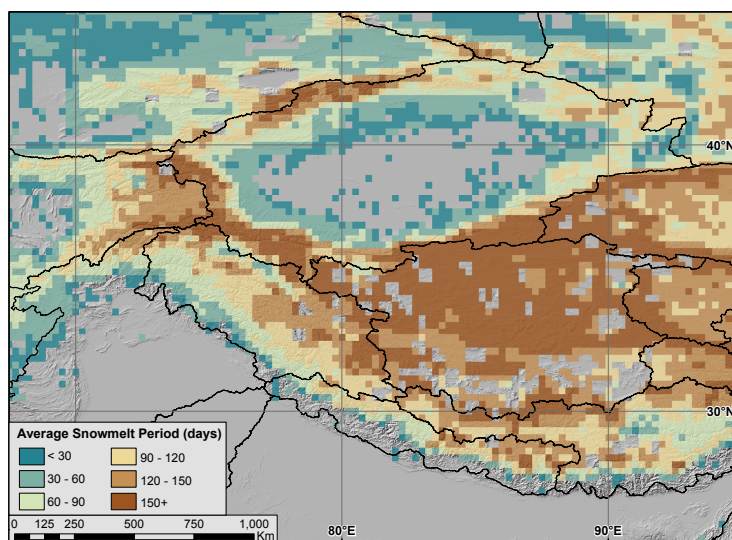
Figure 4. Average snowmelt period across HMA from 1987-2016. Snowmelt period ranges from less than a month to several months, depending on geographic location, elevation, and local climate. Locations with long-term average snowmelt periods less than 20 days are removed. Topographic hillshade in background.
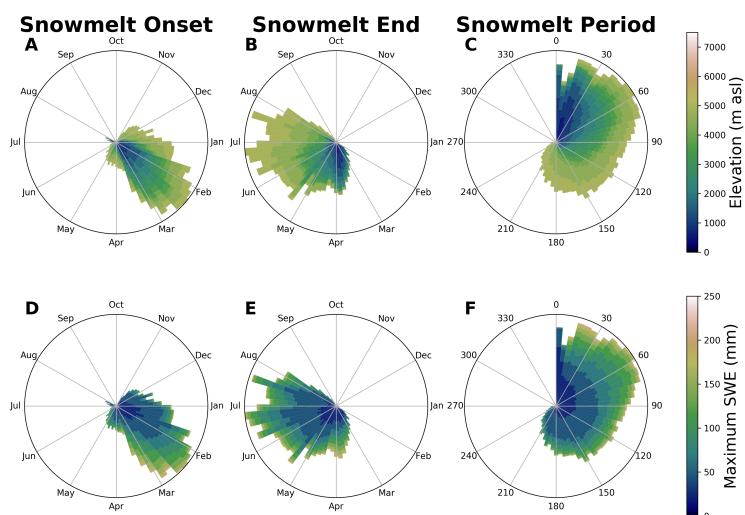
Figure 5. Snowmelt onset (A,D), end (B,E), and period (C,F) for the entire study area, colored by elevation (A-C) and snow depth (D-F) bins. Bin heights indicate relative number of pixels at each day of year (i.e. area). While very short snowmelt periods show a distinct low-elevation, low-SWE bias, in general melt onset and end dates are well distributed throughout elevation zones and SWE amounts.
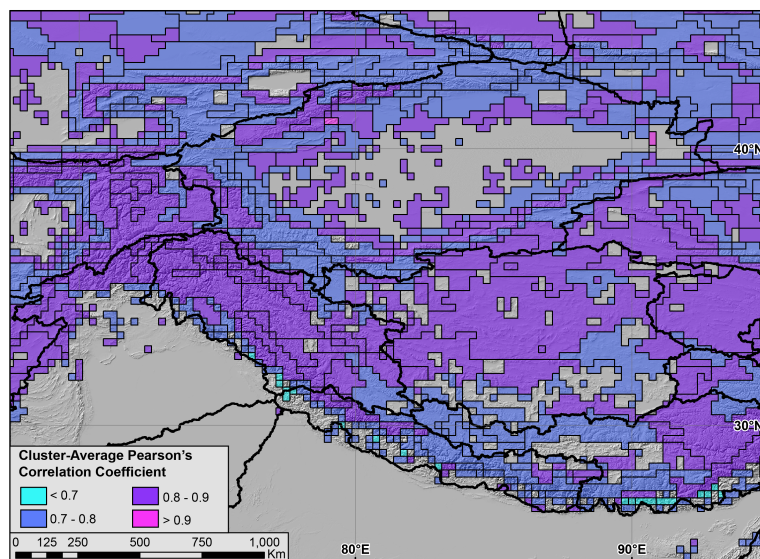
Figure 6. Hierarchical clusters (black outlines), as determined from the rank-order correlation coefficients of the 5-day resampled, merged, and linearly matched XPGR data (1987-2016). Colors indicate cluster-average internal diversity (average Pearson's correlation coefficient between members in the same cluster). Grey areas indicate water bodies, low-SWE areas excluded from the analysis, or areas with irregular PM signals which fail to cluster.
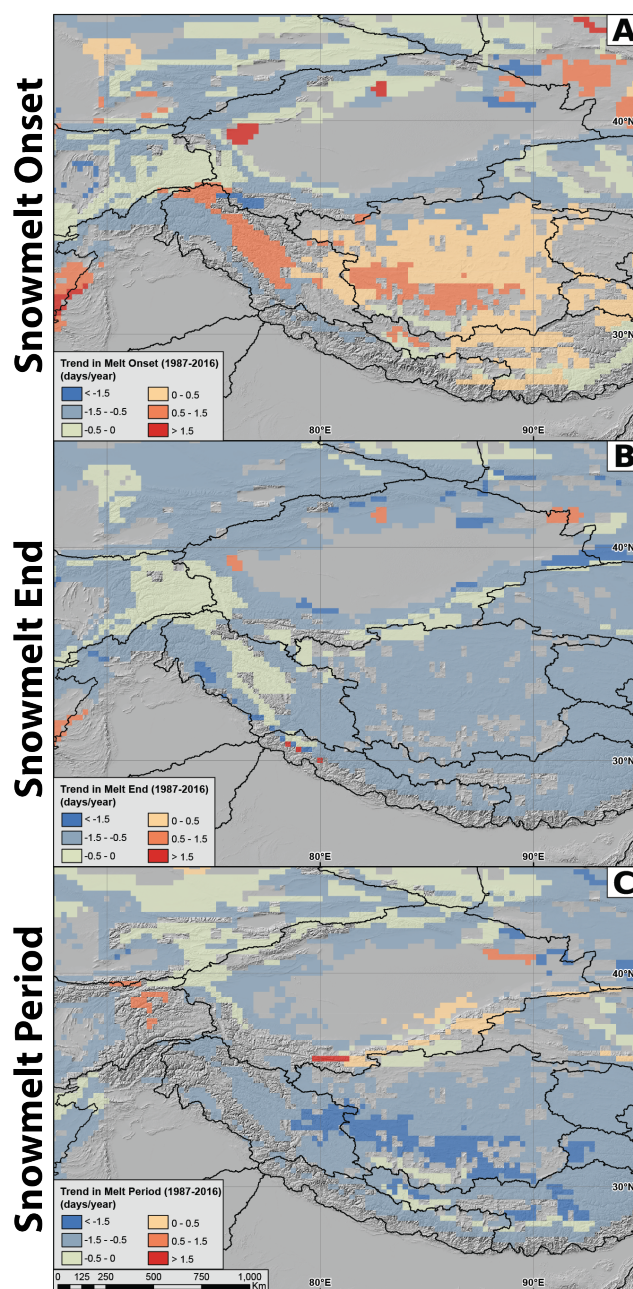
Figure 7. Significant ($p < 0.05$) trends in date of snowmelt (a) onset, (b) end, and (c) period, 1987-2016 for the cluster areas (cf. Fig. 6). The onset of snowmelt is generally moving earlier outside of the Tibetan Plateau, and moving slightly later in a high-elevation zone running from the Karakoram through the Tibetan Plateau interior, as well as parts of the Himalaya. The end of the melt season is moving earlier in the vast majority of HMA, at varying rates. Consequently, snowmelt period is also shrinking in much of HMA, with the exception of parts of the Kunlun Shan along the northern edge of the Tibetan Plateau and small parts of the Pamir.
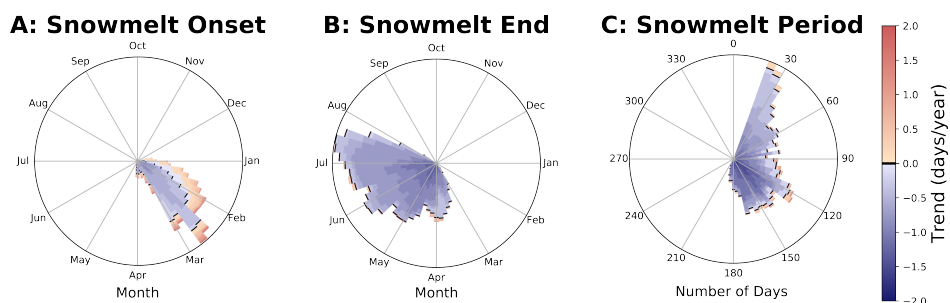
Figure 8. 29-year average snowmelt (a) onset, (b) end, and (c) period, colored by trend (1987-2016), with bin heights indicating relative number of pixels (i.e. area) at each day of year. Black lines indicate zero trend. Data taken only from areas with statistically significant trends ($p < 0.05$, cf. Fig 7). Changes in snowmelt end date are only positive in a few, early onset areas. Negative changes in snowmelt period (shortening) are relatively larger in long snowmelt-period areas.
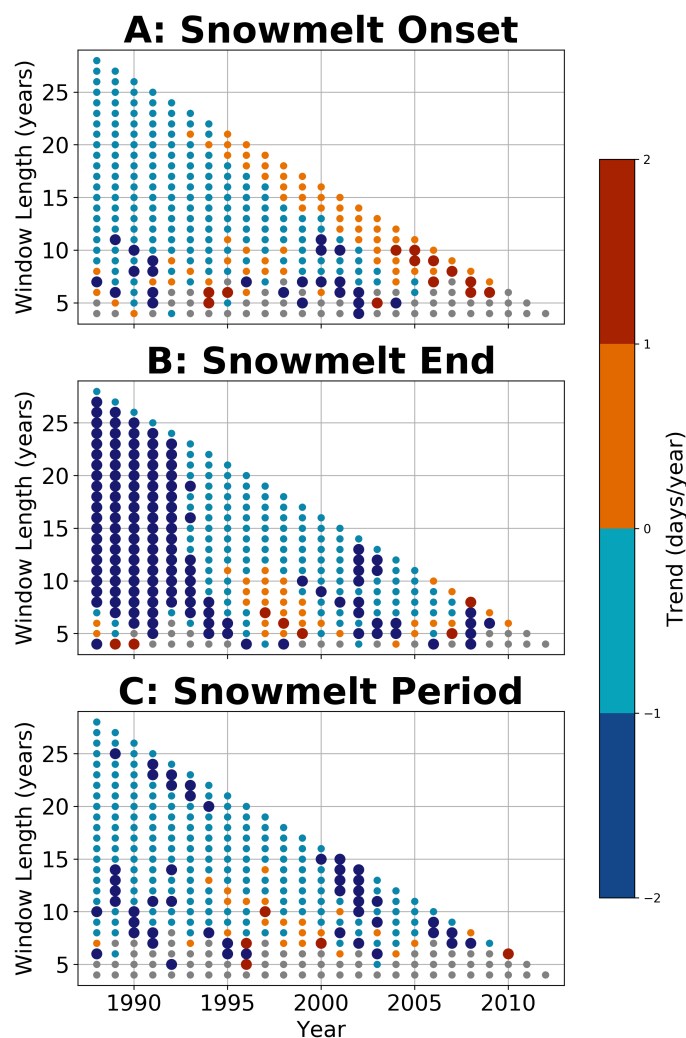
Figure 9. Impact of window length on measured trends in snowmelt (a) onset, (b) end, and (c) period over the entire study area. Each dot represents trends over a single window size (4 to 28 year) and start year (1988-2012) combination. Regressions are performed using the same clusters as shown in Figure 6. Only statistically significant trends ($p < 0.05$) are included in this analysis; gray dots indicate lack of significant trend. Larger dots indicate positive or negative trends larger than 1 day per year. Trends in snowmelt period and snowmelt end dates are almost universally negative regardless of which years the trend is assessed over. Onset dates are positive over short time periods starting in the early 2000s, and negative over earlier time periods and longer time windows.
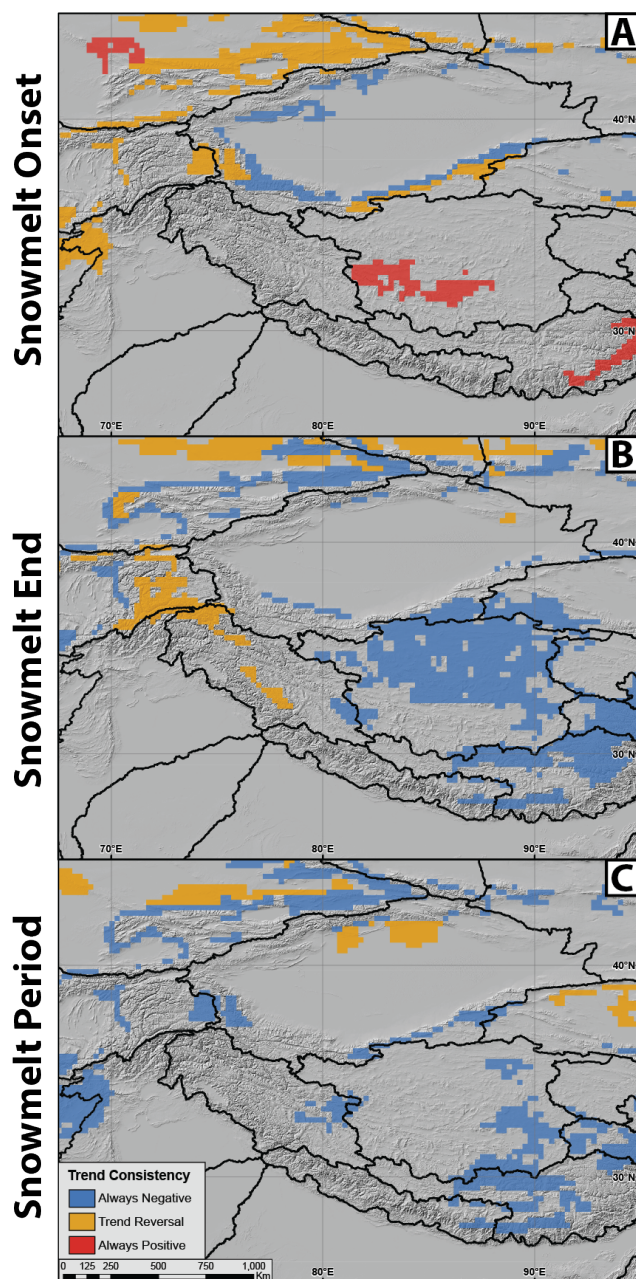
Figure 10. Impact of analysis period (1988-2002 or 2002-2016) on measured trends in snowmelt (a) onset, (b) end, and (c) period. Grey areas indicate lack of statistically significant ($p < 0.05$) trends at one or both analysis periods. Much of HMA lacks significant shorter-term trends in snowmelt onset and snowmelt period, highlighting the complexities and inter-annual variation in snowmelt onset. While much of HMA has maintained a negative trend in snowmelt end throughout both analysis timeframes, a large region running from the Pamir east has had a reversed trend from negative to positive in the last decade. Regression results at both individual timeframes are available in the Supplement (Fig. S4).